JOURNAL OF GEOPHYSICAL RESEARCH, VOL. 113, D13206, doi:10.1029/2007JD009433, 2008

Click Here for Full Article

Quantifying above-cloud aerosol using spaceborne lidar for improved understanding of cloudy-sky direct climate forcing

D. Chand,[1] T. L. Anderson,[1] R. Wood,[1] R. J. Charlson,[1] Y. Hu,[2] Z. Liu,[3] and M. Vaughan[2]

Received 28 September 2007; revised 18 January 2008; accepted 15 February 2008; published 3 July 2008.

[1] Estimates of global mean direct climate forcing by absorbing aerosols located above boundary layer clouds are large, uncertain, and almost entirely unconstrained by observations. Spaceborne lidar offers a new opportunity for global constraints. Here we examine techniques for using liquid water clouds as lidar targets, allowing aerosol optical depth and Ångström exponent to be deduced directly from aerosol effects on light transmission. Two such techniques are examined using data from the Cloud-Aerosol Lidar and Infrared Pathfinder Satellite Observations (CALIPSO). The first is a previously reported method based on measurements of cloud depolarization ratio (DR) at 532-nm wavelength. The second is a new method using measurements of cloud color ratio (CR), which is the ratio of the signal from the cloud at 1064 nm to that at 532 nm. Optical depth retrievals from these two methods compare favorably over the eastern tropical Atlantic Ocean during August 2006, when biomass burning aerosols are frequently advected over marine stratiform clouds. The CR technique is mainly sensitive to fine-mode aerosols and essentially insensitive to clouds and coarse-mode dust. Because anthropogenic aerosol is predominantly found in the fine mode, the CR technique can be used to help identify situations where anthropogenic cloudy-sky direct radiative forcing is occurring. We demonstrate this capability using 6 months data over the eastern tropical Atlantic Ocean.

Citation: Chand, D., T. L. Anderson, R. Wood, R. J. Charlson, Y. Hu, Z. Liu, and M. Vaughan (2008), Quantifying above-cloud aerosol using spaceborne lidar for improved understanding of cloudy-sky direct climate forcing, *J. Geophys. Res.*, *113*, D13206, doi:10.1029/2007JD009433.

1. Introduction

[2] Following the usage in recent review articles [e.g., *Yu et al.*, 2005], we define direct climate forcing (DCF) as the change in radiative flux at the top-of-atmosphere caused by anthropogenic aerosols when considering only the direct interactions between radiation and aerosol particles (indirect forcing involves aerosol-induced changes in clouds and will not be considered here). DCF is dominated by interactions in the shortwave because of the typically small sizes of atmospheric aerosol particles [*Haywood and Shine*, 1997], and its global and regional magnitude is poorly constrained [*IPCC*, 2007; *Schulz et al.*, 2006]. Historically, DCF has been divided into clear-sky and cloudy-sky portions [e.g., *Boucher and Anderson*, 1995; *Haywood et al.*, 1997]. Aerosol retrievals from ground-based radiometers and passive satellite sensors have helped to constrain clear-sky DCF, as summarized by *Yu et al.* [2005]. These same sensors are of limited use for constraining cloudy-sky DCF, and this paucity of empirical constraints is reflected in the uncertainty of current estimates. A recent comparison of nine global models [*Schulz et al.*, 2006] found no agreement even as to the sign of the cloudy-sky DCF, with global annual mean values ranging from −0.16 to +0.34 W/m^2.

[3] Whether the direct effect of aerosols causes heating or cooling of the Earth system depends primarily on the aerosol backscatter coefficient, the aerosol absorption coefficient, and the albedo of the underlying surface [*Charlson and Pilat*, 1969; *Ensor et al.*, 1971; *Chýlek and Coakley*, 1974]. On the basis of this understanding, *Haywood et al.* [1997] pointed out that the most important cloudy-sky direct forcing mechanism is the warming effect of absorbing aerosols located within or above highly reflective boundary layer clouds. This mechanism in turn is most prominently displayed (in those models that exhibit a positive cloudy-sky DCF) over the southeast Atlantic where light-absorbing aerosols from African biomass burning activities are advected over marine stratiform clouds. A positive cloudy DCF in this region has been inferred from airborne measurements of aerosol and cloud properties by *Keil and Haywood* [2003]. The maximum effect occurs around 0–20°S, extending off the coast for 20° or more over the southeast Atlantic Ocean, downwind of the biomass burning areas. However, the calculations by *Keil and Haywood*

[1]Department of Atmospheric Sciences, University of Washington, Seattle, Washington, USA.
[2]NASA Langley Research Center, Hampton, Virginia, USA.
[3]National Institute of Aerospace, Hampton, Virginia, USA.

Copyright 2008 by the American Geophysical Union.
0148-0227/08/2007JD009433$09.00

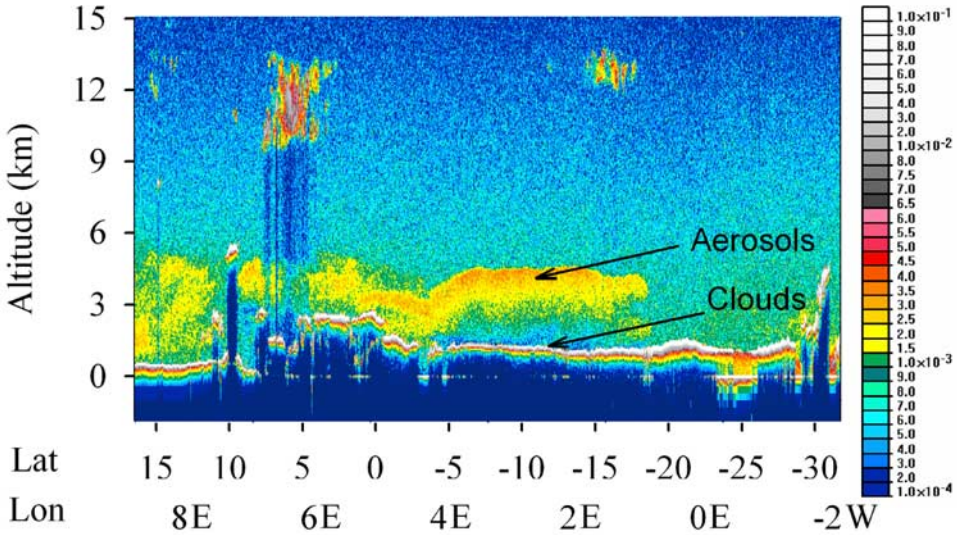

Figure 1. Cloud-Aerosol Lidar with Orthogonal Polarization (CALIOP) total attenuated backscattered signal at 532 nm (units sr^{-1} km^{-1}) observed from 01:17:53 UTC to 01:31:12 UTC on 13 August 2006. Geographical locations of the observation are shown by the altitude, latitude (Lat), and longitude (Lon). Strong backscattering (>0.001 sr^{-1} km^{-1}) is associated with aerosol and/or cloud layers (as indicated by arrows). Low-level clouds (tops 1–1.5 km altitude) are covered by an extensive aerosol layer from approximately 2–18°S. The aerosol layer extends up to almost 5-km altitude. Such a situation occurs very frequently during the biomass burning season (particularly August and September) over the west coast of Africa between the equator and 20°S.

[2003] are sensitive to assumptions about aerosol optical thickness and the albedo of the underlying cloud, both of which were set to the maximum values observed during the campaign. The modeling study by *Schulz et al.* [2006] further emphasizes the uncertainty of cloudy-sky DCF for this region. The various models show annual mean cloudy-sky DCF values in the southeast Atlantic that range from slightly negative to greater than +5 W/m^2. Unraveling these uncertainties will require accurate constraints not only on the optical thickness and radiative properties of the advecting aerosol layers, but also on the radiative properties of the underlying cloud and the extent to which the aerosol and cloud are actually superposed.

[4] Active sensing by spaceborne lidar offers a new opportunity for developing empirical constraints on cloudy-sky DCF. Lidar profiles of attenuated backscatter (e.g., Figure 1) provide unambiguous evidence of aerosol layers located above boundary layer clouds and can be used to quantify some aspects of the problem such as frequency of occurrence and vertical separation. Here we examine two novel techniques for using the 3-channel lidar data from Cloud-Aerosol Lidar and Infrared Pathfinder Satellite Observations (CALIPSO) to provide much stronger constraints on above-cloud aerosols.

[5] Both methods use the underlying cloud as a reflectivity target. Figure 2 illustrates the distribution of low-level clouds judged to be suitable cloud targets by our selection criteria (section 2.4) for two different 16-day periods. Evidently, such clouds are routinely detected by CALIPSO over the entire subtropical and eastern tropical Atlantic Ocean. Thus low clouds over this region provide ample targets for studying elevated aerosol layers.

[6] The depolarization ratio (DR) technique uses polarization information to deduce the optical depth of the overlying atmosphere, as described by *Hu et al.* [2007a]. The color ratio (CR) technique, reported here for the first time, uses dual wavelength information to identify fine-mode aerosols (i.e., aerosols that are likely to be anthropogenic in origin) and to provide an alternate method of deducing optical depth. The goals of this study are to develop practical methodologies for exploiting these promising new techniques and to examine their strengths and limitations in order to facilitate their use in improved global quantification of cloudy-sky DCF.

2. Methods

2.1. CALIOP Basics

[7] The CALIPSO satellite was launched 28 April 2006 for a nominal 3-year mission as part of the A-Train constellation of satellites [*Stephens et al.*, 2002]. *Winker et al.* [2002] provide a detailed description of the CALIPSO instruments and *Winker et al.* [2007] assess instrument performance over the first year of operation.

[8] The primary CALIPSO instrument is the Cloud-Aerosol Lidar with Orthogonal Polarization (CALIOP). CALIOP's laser transmits linearly polarized light simultaneously at 532 nm and 1064 nm at a pulse rate of 20.16 Hz, and its receiver measures backscatter intensity at 1064 nm and 532 nm, with the latter divided into two orthogonally polarized components, giving a total of three channels. CALIOP observes both clouds and aerosols at high spatial resolution as shown, for example, in Figure 1. Level-1 CALIOP data consist of calibrated, geolocated, vertical

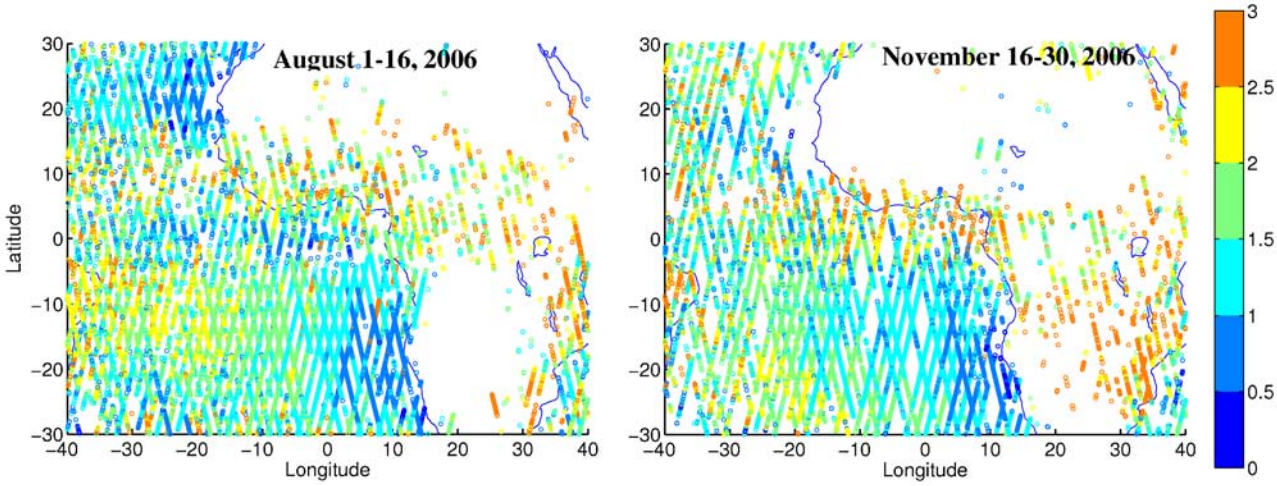

Figure 2. Map showing locations where CALIOP observes low-level (<3 km) clouds as determined by the Level-2 cloud mask (CAD score > 90, SNR > 2) for 1–16 August 2006 (left) and 16–30 November 2006 (right). The color indicates the height of the top of the cloud layers. The Cloud-Aerosol Lidar and Infrared Pathfinder Satellite Observations (CALIPSO) repeat the ground track sampling approximately in 16 days so that the map serves as a qualitative demonstration of the prevalence of low clouds over the eastern Atlantic Ocean.

profiles of total attenuated backscatter at 532 nm, β'_{532}, perpendicularly polarized attenuated backscatter at 532 nm, $\beta'_{p,532}$, and total attenuated backscatter at 1064 nm, β'_{1064}. From the surface to 8 km, the vertical resolution is 30 m, and the nominal horizontal resolution is 1/3 km. (More specifically, laser pulses with a footprint of ~70 m at sea level are spaced 333 m apart.) The β'_{532} channel is calibrated by examining molecular scattering returns from the midstratosphere, assumed to be particle-free, at night. The other two channels are calibrated with respect to β'_{532}. Calibration of $\beta'_{p,532}$ uses an onboard depolarizer periodically inserted upstream of the polarization beam splitter. Calibration of β'_{1064} uses returns from optically thick cirrus clouds that are sufficiently high that the beam does not pass through aerosol layers above them. Such cirrus are assumed to backscatter with equal efficiency at the two wavelengths in accordance with surface lidar observations [*Beyerle et al.*, 2001]. Data quality is considerably better at night because there is no background noise from scattered solar radiation and because the primary calibration of the β'_{532} channel is continually updated. Calibration accuracy of all channels under all conditions is being assessed through ongoing validation activities including this study (e.g., the CALIPSO-CloudSat Validation Experiment (CCVEX) during July and August 2006 [*McCubbin et al.*, 2006].)

[9] Level-2 data files provide the location and properties of atmospheric "features," identified at averaging scales corresponding to horizontal resolutions from 1/3 km to 80 km. A feature (or layer) is identified as a detectable departure from the expected profile for pure molecular backscattering (CALIPSO Level-2 Algorithm Theoretical Basis Document, NASA, available at http://www-calipso.larc.nasa.gov/resources/project_documentation.php, henceforth ATBD, 2007). In addition to vertical and horizontal location, CALIOP provides three fundamental pieces of information for each identified layer, corresponding to the vertical integrals (over the layer) of each lidar channel. As discussed in sections 2.2 and 2.3, it is useful to express these three basic measurements as layer-integrated values of β'_{532}, depolarization ratio, and color ratio (see section 2.3 for definitions of these latter two quantities). In contrast to these directly measured quantities, advanced products like layer optical depth require additional, often assumed information and a retrieval algorithm. In order to introduce the retrieval methods discussed herein, we now discuss two distinct approaches to the retrieval of optical depth.

2.2. Optical Depth by Forward Iteration Versus Transmission Methods

[10] Layer optical depth, τ_{layer}, is a Level-2 CALIPSO product provided for each identified feature. (Note, however, that retrievals of τ_{layer} are not provided in the version 1 data products used herein.) The standard retrieval method is an iterative, forward calculation that requires knowledge of the extinction-to-backscatter ratio, S, of the scattering material within the layer (ATBD, 2007). Because S is, in general, uncertain and because the standard retrieval is highly sensitive to errors in S [see, e.g., *Stephens et al.*, 2001], a preferred retrieval method is to use a target of known reflectivity on the under side of the layer. In that case, the signal from this target is reduced in direct proportion to the two-way transmissivity of laser light through the intervening atmosphere. Such "transmission" methods [*Young*, 1995] tend to be simpler and more accurate, largely because they do not require knowledge of S. Unfortunately, suitable lidar targets are hard to find. The only established technique uses "clear air"; that is, portions of the lidar profile assumed to be free of particles. For spaceborne lidar, this requires that a region of particle-free air can be identified beneath the aerosol or cloud layer to be analyzed: a fairly

unusual situation except for thin cirrus. Moreover, 180° backscattering by air molecules is rather weak at the midvisible CALIOP wavelength (532 nm) and is much too weak to be useful at the near-infrared wavelength (1064 nm). Optical depths obtained by the clear-air transmission method will be included among the CALIOP Level-2 data products and, when available, these will provide a valuable comparison to optical depths obtained by the standard forward iteration. However, these data are too sparse to be used for constructing regional climatologies of lower-tropospheric clouds or aerosols.

[11] Thus, a transmission technique that used a bright and commonly available lidar target would be extremely useful. This paper examines two possible ways of using horizontally extensive liquid water clouds for this purpose. Such clouds are common in the boundary layer. The annual mean global low cloud coverage is approximately 40% [e.g., *Rossow and Schiffer*, 1999], and these clouds provide an enormous lidar signal at both CALIOP wavelengths. Moreover, successful application of such techniques would provide data of direct relevance to the problem of cloudy-sky DCF.

2.3. Transmission Techniques Using Liquid Water Clouds

[12] We describe these techniques in terms of products available in the CALIOP Level-2 files. As mentioned in section 2.2, Level-2 products include the altitude range and three directly measured quantities for each layer. These consist of three extensive properties, corresponding to the three lidar channels. It is convenient to represent these as one extensive property and two ratios; that is, (1) layer-integrated attenuated backscatter at 532 nm, γ'_{532}, (2) layer-integrated attenuated depolarization ratio at 532 nm, δ'_{532}, which is the ratio of the perpendicular to the parallel components of γ'_{532}, and (3) layer-integrated attenuated color ratio, χ', which is the ratio of integrated attenuated backscatter at 1064 nm (γ'_{1064}) to 532 nm (γ'_{532}). The two ratios, δ'_{532} and χ', form the basis of the two retrieval techniques. Note that throughout this manuscript, and in accordance with the CALIPSO ATBD, primed quantities indicate that the property being considered has not been corrected for attenuation by any aerosol or cloud particles that might be present above the layer in question.

2.3.1. Depolarization Ratio Method

[13] *Hu et al.* [2007a] showed that the values of γ'_{532} and δ'_{532} obtained for opaque water clouds can be used to deduce the optical depth ($\tau_{\mathrm{top,DR}}$) of overlying aerosol and/or cloud layers. As an initial test, *Hu et al.* [2007a] examined a case of thin cirrus overlying thick, marine boundary layer stratus and showed that $\tau_{\mathrm{top,DR}}$ retrievals were consistent with retrievals from the traditional transmission technique in which particle-free air beneath the cirrus was used as the lidar target. This section reviews the nomenclature and physics of the depolarization ratio (DR) technique.

[14] An "opaque" cloud or aerosol layer is one that fully attenuates the lidar beam. For Nd:YAG-based backscatter lidars similar to CALIOP, complete attenuation of the signal occurs at single scattering optical depths of ~3 [*McGill et al.*, 2002]. Boundary layer clouds frequently exceed this optical depth such that opaque, low-level clouds are common in the CALIPSO data set. Let γ'_{water} represent, γ'_{532} for an opaque liquid water cloud and let $\gamma'_{\mathrm{water,unobstructed}}$ represent the theoretical value of γ'_{water} if it were viewed by CALIOP through an atmosphere with negligible nonmolecular attenuation. (Level-2 layer products are corrected for clear-air molecular attenuation above the layer.) In addition, let $\gamma'_{\mathrm{water,SS}}$ represent the theoretical, single scattering value of γ'_{water}; that is, the value that would be measured by a lidar with an infinitely narrow field of view such that only 180° backscattered photons, and no multiply scattered photons, were detected. The relationship between these quantities was deduced by *Platt et al.* [1999] as follows,

$$\gamma'_{\mathrm{water,SS}} = \gamma'_{\mathrm{water}}\eta_{\mathrm{c}} \tag{1a}$$

$$\gamma'_{\mathrm{water,SS,unobstructed}} = \gamma'_{\mathrm{water,unobstructed}}\eta_{\mathrm{c}} = (2S_{\mathrm{c}})^{-1} \tag{1b}$$

where η_{c} (between 0 and 1) is the cloud multiple scatter factor (which depends upon both cloud properties and lidar field of view) and S_{c} is the cloud extinction-to-backscatter ratio.

[15] For liquid water clouds with droplets smaller than about 50 μm, S_{c} is well known and narrowly constrained to about 19 sr [*Pinnick et al.*, 1983; *O'Connor et al.*, 2004; *Hu et al.*, 2006] at a wavelength of 532 nm, and *O'Connor et al.* [2004] show negligible differences between S_{c} at 532 and 1064 nm. Recently, *Hu et al.* [2006, 2007b] used three-dimensional radiative transfer calculations to show that, for the geometry of a spaceborne lidar like CALIOP, the multiple scattering factor, η_{c}, is strongly related to the cloud depolarization ratio, δ'_{water}. This relationship can be approximated by

$$\eta_{\mathrm{c}} \approx \left(\frac{1-\delta'_{\mathrm{water}}}{1+\delta'_{\mathrm{water}}}\right)^2 \tag{2}$$

[16] A required assumption of the DR method is that δ'_{water} is negligibly affected by whatever aerosol or thin cloud layers lie between the liquid water cloud and the lidar instrument. If so, then the CALIOP data provide a measurement of $\gamma'_{\mathrm{water,SS}}$ (via equations (1a) and (2)) which can be compared to either a theoretically or empirically determined value of $\gamma'_{\mathrm{water,SS,unobstructed}}$ (via equation (1b)) in order to deduce the amount of attenuation caused by the intervening atmosphere. Making use of the Beer-Lambert law governing transmission of light through an attenuating medium, we have

$$\frac{\gamma'_{\mathrm{water,SS}}}{\gamma'_{\mathrm{water,SS,unobstructed}}} = T^2 = \exp\left(-2\tau_{\mathrm{top,DR}}\right) \tag{3}$$

where T^2 is the two-way transmittance of the nonmolecular atmosphere above the cloud. Solving for optical depth gives

$$\tau_{\mathrm{top,DR}} = -\frac{1}{2}\ln\left(\frac{\gamma'_{\mathrm{water,SS}}}{\gamma'_{\mathrm{water,SS,unobstructed}}}\right) \tag{4}$$

Table 1. Data Symbols, Sources, and Uncertainties for Parameters Used to Retrieve τ_{top} by Both CR and DR Methods[a]

Method	Parameter	Source	Value and Uncertainty
DR Method	γ'_{water}	Level-2 data	variable
	δ'_{water}	Level-2 data	variable
	$[\gamma'_{water,SS,unobstructed}]$[b]	[a priori][c]	[0.026 ± 0.0015]
	$\gamma'_{water,SS,unobstructed}$	empirical[d]	see Table 2
CR Method	χ'_{water}	Level-2 data	variable
	$[\chi'_{water,unobstructed}]$[b]	[a priori][e]	[1.0 ± 0.15]
	$\chi'_{water,unobstructed}$	empirical[d]	see Table 2
	$[å]$	[a priori][f]	[2.0 ± 0.4]

[a]CR is color ratio; DR is depolarization ratio.
[b]Not used in this study, but included for completeness.
[c]See section 2.3.1.
[d]This work.
[e]See section 2.3.2.
[f]See section 2.5.2.4.

[17] Rearranging terms, we can express the DR formula for above-cloud optical depth (at 532 nm) in terms of CALIOP Level-2 products as follows,

$$\tau_{top,DR} = -\frac{1}{2}\ln\left(\frac{\gamma'_{water}}{\gamma'_{water,SS,unobstructed}}\left(\frac{1-\delta'_{water}}{1+\delta'_{water}}\right)^2\right) \quad (5a)$$

$$= -\frac{1}{2}\ln\left(2S_c\gamma'_{water}\left(\frac{1-\delta'_{water}}{1+\delta'_{water}}\right)^2\right) \quad (5b)$$

Note that $\gamma'_{water,SS,unobstructed}$ acts as a calibration constant for the DR method. The theoretical or expected value of this constant, as shown by equations (1b) and (5b), is $(2S_c)^{-1}$, or 0.026 sr^{-1} if we set S_c to its observed value of 19 sr (see Table 1). Using this value to retrieve $\tau_{top,DR}$, as in equation (5b), relies on (1) the physical accuracy of the Platt relationship (equation (1b)) and of the assumed value of S_c, (2) the accuracy of the lidar calibration at 532 nm (both the parallel and perpendicular channels), and (3) the accurate correction for molecular attenuation above the cloud in the Level-2 cloud layer products. Alternatively, $\gamma'_{water,SS,unobstructed}$ can be determined empirically, as described in section 2.5.2, by assembling data from opaque, liquid water clouds with no overlying clouds or aerosols.

2.3.2. Color Ratio Method

[18] We introduce a new method for identifying and quantifying fine-mode aerosol layers overlying liquid water clouds. Because it uses attenuated color ratio, χ', we dub this the color ratio (CR) method. In this section we present the nomenclature and physical basis of this method.

[19] The size distributions of aerosol particles in the atmosphere generally consist of two modes: a mechanically produced coarse mode and a fine mode produced by combustion and/or gas-to-particle conversion [*Whitby et al.*, 1972]. Over the visible to near-IR wavelength region, fine-mode aerosols exhibit optical extinction that is strongly wavelength dependent, whereas coarse-mode aerosols and cloud particles exhibit little or no wavelength dependence [*van de Hulst*, 1981]. To represent this optical behavior, we define an Ångström exponent [*Ångström*, 1929], $å$, in terms of the two CALIOP wavelengths, i.e.,

$$å = \frac{-\ln\left(\frac{\tau_{1064}}{\tau_{532}}\right)}{\ln\left(\frac{1064}{532}\right)} \quad (6)$$

where τ_i represents optical depth at wavelength i. For fine-mode aerosols, which typically have volume equivalent diameters in the range 100–400 nm, $å$ is in the range 1.5–3 [e.g., *Seinfeld and Pandis*, 1998].

[20] Let χ'_{water} represent χ' for a liquid water cloud (note that the CR method does not necessarily require opaque clouds, as does the DR method) and let $\chi'_{water,unobstructed}$ represent the value of χ'_{water} if viewed by CALIOP through an atmosphere with negligible nonmolecular attenuation. From the above discussion it follows that the presence of fine-mode aerosol overlying a cloud will cause stronger attenuation of the reflected laser light at 532 nm than at 1064 nm which, in turn, will cause an increase in χ'_{water}. In contrast, thin clouds or coarse-mode aerosol above the cloud will cause little or no change in χ'_{water}. Therefore, χ'_{water} can be used to identify the presence of fine-mode aerosol above clouds.

[21] The increase in χ'_{water} caused by overlying aerosol is a function of the aerosol optical depth and the aerosol Ångström exponent. For each of the two wavelengths, the signal from the cloud in terms of integrated attenuated backscatter, γ'_{water}, will be reduced by the two-way transmittance of the atmosphere (T_{532} and T_{1064} for the two CALIOP wavelengths). Therefore, invoking the Beer-Lambert law as in equation (3), we see that the observed cloud color ratio divided by the unobstructed cloud color ratio will be

$$\frac{\chi'_{water}}{\chi'_{water,unobstructed}} = \left(\frac{T_{1064}}{T_{532}}\right)^2 = \frac{\exp(-2\tau_{top,1064})}{\exp(-2\tau_{top,532})} \quad (7)$$

[22] Solving for $\tau_{top,532}$ and renaming this $\tau_{top,CR}$ for consistency with equation (4) leads to the formula for overlying optical depth at 532 nm from the CR method:

$$\tau_{top,CR} = \frac{1}{2}\ln\left(\frac{\chi'_{water}}{\chi'_{water,unobstructed}}\right)\frac{1}{(1-2^{-å})} \quad (8)$$

[23] Just as $\gamma'_{water,SS,unobstructed}$ acts as a calibration constant for the DR method, $\chi'_{water,unobstructed}$ is a calibration constant for the CR method. The theoretical value of this constant is 1. Using this value to retrieve $\tau_{top,CR}$ relies on (1) the physical assumption that both 180° backscattering and multiple scattering exhibit no wavelength dependence for liquid water clouds, (2) the accuracy of the lidar calibration (1064-nm calibration with respect to that at 532 nm), and (3) the accurate correction for molecular attenuation above the cloud in the Level-2 cloud layer products. Alternately, these assumptions can be circumvented by determining $\chi'_{water,unobstructed}$ empirically, as described in section 2.5.2.

2.3.3. Combination of the DR and CR Method to Estimate Ångström Exponent

[24] To recap, the DR method requires opaque target clouds, responds to a reduction in $\gamma'_{water,SS}$ compared to the value for unobstructed clouds, and retrieves above-cloud optical depth regardless of the nature of the overlying material. The CR method does not necessarily require opaque clouds, responds to an increase in χ'_{water} compared

Table 2. Key Parameters in the DR and CR Methods Determined Using Unobstructed Low Clouds Over a Pristine Region of the Eastern Atlantic Ocean for the Month of November 2006[a]

	$\gamma'_{\text{water_SS_unobstructed}}$			$\chi'_{\text{water_unobstructed}}$		
Time	Mean (Median)	SD	DL_{DR} (τ_{top})	Mean (Median)	SD	DL_{CR} (τ_{top}) N
Target Cloud Screening Criteria: Altitude < 3 km, *CAD > 90, Horizontal Averaging = 5* km, *SNR > 2*						
Day	0.022 (0.022)	0.004	0.013 (0.27)	1.14 (1.15)	0.055	1.28 (0.07) 459
Night	0.030 (0.030)	0.003	0.024 (0.12)	1.11 (1.11)	0.062	1.25 (0.08) 930
Target Cloud Screening Criteria: Altitude < 3 km, CAD > 90, Horizontal Averaging = 5 km, SNR > 2, Opacity Flag = 1						
Day	0.023 (0.022)	0.002	0.017 (0.12)	1.14 (1.16)	0.053	1.28 (0.07) 367
Night	0.030 (0.030)	0.002	0.025 (0.10)	1.10 (1.11)	0.060	1.25 (0.08) 805

[a]The calculations are made using unobstructed χ'_{water}, γ'_{water} and δ'_{water} cases (tops< 3 km) with screening criteria discussed in section 2.4. Region of the eastern Atlantic Ocean is 30–20°S, 0–10°W. The Opacity Flag criterion is omitted in the top row in order to show its effect on sample number and variability of the calibration constants. Means, medians, and standard deviations (SD) of the distributions of unobstructed attenuated backscatter $\gamma'_{\text{water,SS,unobstructed}}$ and unobstructed color ratio $\chi'_{\text{water,unobstructed}}$ are given for day and night separately. On the basis of the distributions of unobstructed properties, a detection limit (DL) can be determined for the DR and CR methods. The DL is the critical value of $\gamma'_{\text{water,SS}}$ or χ'_{water} for which we reject the hypothesis (at the 99% level) that the air above the cloud contains no aerosol layer. The DL is calculated (assuming a normal distribution of errors) as $DL_{DR} = \bar{x} - 2.33\sigma$ (DR method) and $DL_{CR} = \bar{x} + 2.33\sigma$ (CR method) where 2.33 represents the critical t_value for a large number of degrees of freedom (greater than 100). Thus, for the DR method, if $\gamma'_{\text{water,SS}} < DL_{DR}$ we classify the cloud as having an elevated aerosol layer above (for the CR method χ'_{water} must exceed DL_{CR}). The corresponding DL with respect to τ_{top} is also given for both methods. The number of data points, N, is the same for both methods, since the same screening criteria are applied.

to the value for unobstructed clouds, and is primarily sensitive to fine-mode aerosols.

[25] To retrieve above-cloud optical depth, the CR method requires a priori knowledge of $\mathring{a}$. In situations where the aerosol type is well known (e.g., the African biomass burning cases considered here), $\mathring{a}$ may be well constrained. In general, however, this is not the case, especially where the aerosol consists of an unknown mixture of fine and coarse components. Thus, it may be useful to combine the two techniques wherein the CR method identifies the presence of fine-mode aerosol, the DR method determines aerosol optical depth, and, using this as an input, the CR method determines the wavelength dependence of aerosol optical depth. Rearranging equation (8), the expression for $\mathring{a}$ is

$$\mathring{a} = -\frac{1}{\ln(2)} \ln\left(1 - \frac{1}{2\tau_{\text{top,DR}}} \ln\left[\chi'_{\text{water}} \Big/ \chi'_{\text{water,unobstructed}}\right]\right) \qquad (9)$$

Section 3.2 describes application of equation (9) for determination of the Ångström exponent using the combination of the DR and CR methods.

2.4. Data Selection

[26] Our analysis is based on daytime and nighttime CALIOP Level-2, Version 1, 5-km resolution cloud layer products over the eastern Atlantic Ocean (30°S to 30°N, 40°W to 40°E) during the 6-month period from June–November 2006. Version 1 is the first public release of Level-2 data and does not yet contain advanced retrieval products such as aerosol or cloud optical depth. It does contain basic retrievals of layer top and bottom altitudes, vertical integrals of the three lidar channels, and layer categorization as either cloud or aerosol. We select lower-tropospheric clouds (cloud top below 3 km) and confine our analysis to the tropics in order to assure that all target clouds are composed of liquid water.

[27] To investigate the properties of unobstructed cloud layers, we select cases with thick, low cloud from a relatively nonpolluted portion of the study region (20–30°S, 0–10°W, November 2006) and we remove all cases in which the Level-2 data indicate overlying cloud or aerosol layers. This "pristine" data subset is used to develop empirical estimates of the calibration constants, $\chi'_{\text{water,unobstructed}}$ and $\gamma'_{\text{water,SS,unobstructed}}$, and their uncertainties (see section 2.5.2, Table 2, and Figure 3.)

[28] To compare the two methods of retrieving τ_{top}, we focus on a region (5–15°S, 0–10°E) and time (August 2006) when maximum biomass burning aerosol was observed within our study area. According to *Klein and Hartmann* [1993], mean low cloud cover for this region in August ranges from 60 to 75%. Results from this "polluted" data subset are presented in section 3.1.

[29] Implementing either the CR or DR method requires the identification of suitable cloud targets. Thin or patchy clouds, for example, would violate a basic assumption of the DR method and might cause problems for the CR method as well. These thin or patchy clouds can be effectively identified and removed using Level-1 data; however, incorporating Level-1 data into our regional- and seasonal-scale analysis would require approximately 50 times the computational resources we have currently dedicated to this project. Therefore, we have developed screening criteria that use 5-km Level-2 data only. Application of these criteria to unobstructed clouds (section 2.5.2) allows us to evaluate their effectiveness. Screening criteria available in the Level-2 product files include horizontal averaging (the horizontal resolution at which the cloud was detected), the Cloud-Aerosol-Discrimination (CAD) score, the Opacity Flag, and the reported uncertainties in the three basic layer properties: γ'_{water}, δ'_{water}, and χ'_{water}.

[30] The CAD algorithm (ATBD, 2007) [*Liu et al.*, 2004] separates clouds and aerosols on the basis of empirically determined, altitude-dependent histograms of their optical properties (backscatter intensity and its spectral dependence). If the observed properties of a layer fall in a region of parameter space where the histograms overlap, the more likely classification is selected and the CAD score indicates the probability that the classification is correct. Many layers fall outside this overlap region and, thus, receive a CAD score of magnitude 100 (complete confidence). In this study cloud layers are selected as reflectivity targets only when the reported CAD score is 90 or higher. Note that the CAD score in Version 1 is not necessarily an accurate confidence estimate since the histograms of cloud and aerosol properties are based on prelaunch data from airborne lidar. These

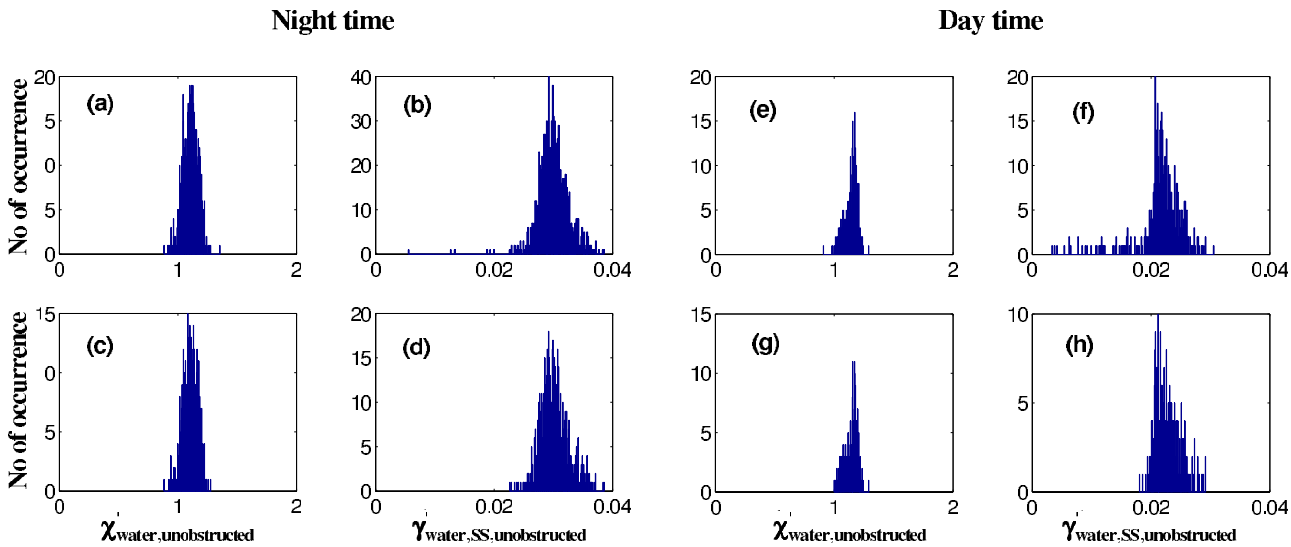

Figure 3. Histograms showing the frequency distribution of $\gamma'_{\text{water,SS,unobstructed}}$ (a, c, e, and g) and $\chi'_{\text{water,unobstructed}}$ (b, d, f, and h) for a relatively pristine region (20–30°S, 0–10°W) during November 2006. Data selection criteria are described in section 2.5.2. Figure 3, top (a, b, e, and f), shows results without the Opacity Flag criterion, while Figure 3, bottom (c, d, g, and h), includes this criterion. Figure 3, left (a–d) and Figure 3, right (e–h) are for nighttime and daytime, respectively. For a statistical summary of these distributions, see Table 2.

are currently being revised in light of experience with actual CALIOP data.

[31] Level-2 reported uncertainties in γ'_{water}, δ'_{water}, and χ'_{water} reflect random shot noise estimated for each 5-km retrieval block, as described by *Liu et al.* [2006]. We select target clouds only if the relative uncertainty in all three parameters is less than a threshold. For convenience, we define this threshold in terms of signal-to-noise (SNR): the inverse of relative uncertainty. We find that the relative uncertainty of δ'_{water} is almost always the largest of the three such that the screening criterion primarily operates on this parameter. We require that SNR for all three parameters be at least 2.

[32] In some cases, cloud features reported in the 5-km layer file required 20-km or even 80-km horizontal averaging in order to be detected. These would be very thin or broken clouds not suitable to serve as reflectivity targets. We remove such cases by requiring that the horizontal averaging parameter be 5 km.

[33] The most important parameter in our selection scheme is the Opacity Flag, which is set to 0 whenever the surface can be detected and to 1 whenever the lidar beam is judged to be fully attenuated above the surface. Table 2 and Figure 3 illustrate the effect of this criterion on data used to determine the calibration constants (see section 2.5.2), and Figure 4 illustrates the effect on retrievals of τ_{top} (see section 3.1.)

2.5. Algorithm Parameter Estimation and Uncertainties

[34] Uncertainties are estimated using the standard method of propagation of errors:

$$\delta F = \sqrt{\sum_{i=1}^{n} \left(\frac{\partial F}{\partial x_i} \delta x_i \right)^2} \tag{10}$$

where F represents $\tau_{\text{top,DR}}$, $\tau_{\text{top,CR}}$ or $\mathring{a}$ derived from equations (5), (8), and (9), respectively, x_i is the ith independent variable of the function F, and n is the number of variables. In this study all uncertainties are given at the 1σ level.

[35] Each method of retrieving τ_{top} and its uncertainty requires knowledge of three parameters and their uncertainties. As shown in Table 1, these parameters divide into three categories: CALIOP Level-2 data, empirically determined calibration constants, and the Ångström exponent, $\mathring{a}$, which appears in the CR method as an a priori constant. (The calibration constants can also be determined a priori; however, that is not our approach.) Reported uncertainties in Level-2 data involve random error and are discussed in section 2.5.1. Uncertainties in calibration constants and $\mathring{a}$ involve systematic error and are discussed in section 2.5.2.

2.5.1. Level-2 Data and Random Error

[36] The DR method (equation (5)) involves two Level-2 CALIOP variables γ'_{water} and δ'_{water} while the CR method involves just one, χ'_{water}. In all three cases, parameter uncertainties are provided in the data files. The reported uncertainties are calculated subsequent to averaging the 15 shots within each 5-km retrieval block and, therefore, do not provide information on sub-5-km variability. What they do provide are estimates of random, shot-noise error specific to each 5-km block [*Liu et al.*, 2006]. Because the source of uncertainty is random error, it can be reduced by further averaging.

[37] To determine the random error in $\tau_{\text{top,DR}}$, we propagate uncertainties in γ'_{water} and δ'_{water} using equation (10) applied to equation (5a); similarly, to determine random error in $\tau_{\text{top,CR}}$, we propagate uncertainties in χ'_{water} using equation (10) applied to equation (8). For the month (August 2006) and region (5–15 °S, 0–10 °E) of maximum

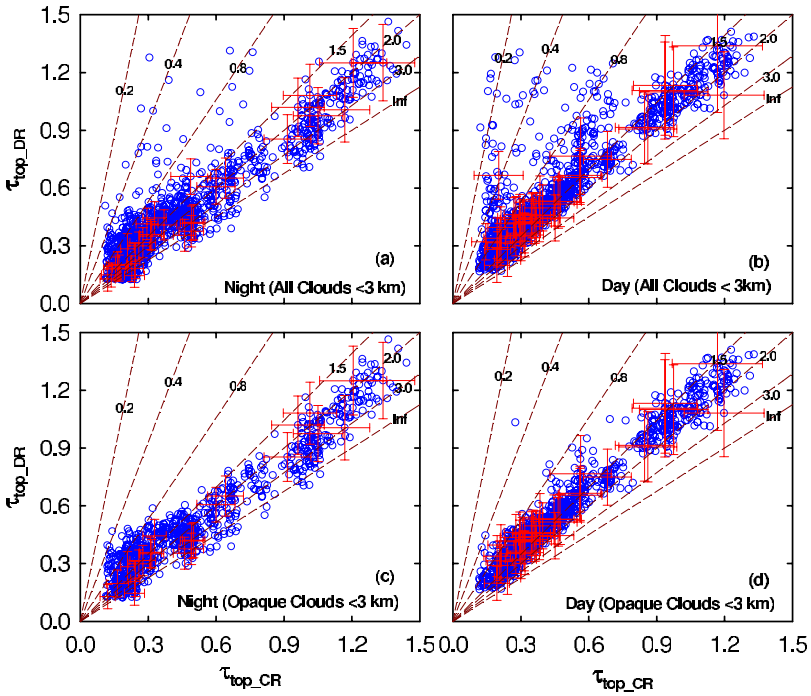

Figure 4. Comparison of aerosol optical thickness calculated using the color ratio (CR) method ($\tau_{top,CR}$) with that from the DR method ($\tau_{top,DR}$) for nighttime (left) and daytime (right) CALIOP observations for a highly polluted region: 5–15°S, 0–10°E during August 2006. As in Figure 3, Figure 4, top (a and b) shows results without the Opacity Flag criterion, while Figure 4, bottom (c and d) includes this criterion. The error bars show the 1σ uncertainties for each method, the quadratic sum of random and systematic errors as discussed in section 3. For visual clarity, error bars are plotted for a only 3% of the data points. Data where either the DR or CR method indicates values below the detection limit (see sections 2.5.1 and 2.5.2) are not shown. The dashed lines show the Ångström exponent $\mathring{a}$ from equation (11).

biomass burning influence, the median random error in $\tau_{top,DR}$ is 0.08 during the night and 0.12 during the day. Uncertainties in both γ'_{water} and δ'_{water} contribute significantly to these errors but in general (and for both day and night), the error contribution from the polarization ratio δ'_{water} outweighs that from γ'_{water} by roughly a factor of two. For the same month and region, the median random error in $\tau_{top,CR}$ is 0.06 during the night and 0.09 during the day. Thus, the random errors for the CR method are seen to be similar, but smaller by a factor of about two thirds. This reflects the common error source associated with the 532-nm channel and the fact that the 1064-nm channel has much smaller random error than the depolarization channel.

2.5.2. Calibration Constants and Systematic Error

[38] Unobstructed low clouds can be found on almost every orbit and are readily identified by the CALIOP feature finder. They offer an attractive approach to determining the calibration constants required in the retrieval of τ_{top} for two reasons. First, this approach should largely compensate for any errors in the calibration of the three CALIOP channels. Second, it provides an empirical means of assessing the detection limit and the systematic error of the optical depth retrievals.

[39] To generate a large sample of unobstructed clouds, we select a month of data from a remote 10° × 10° (30–20°S, 0–10°W) region, and we screen these data for the occurrence of high cloud or aerosol layers located above the target cloud. (In other words, we require that the target cloud be the only layer identified in the entire atmospheric column.) The resulting statistics on the calibration constants for each method are shown in Table 2 and Figure 3. We also use this exercise to show the effect of the Opacity Flag criterion.

2.5.2.1. Day Versus Night

[40] Table 2 shows that the mean values of both calibration constants differ substantially between day and night. These differences likely indicate uncorrected drift in lidar calibration during the day associated with solar heating of the instrument. Improving the daytime calibration of all three CALIOP channels is an ongoing priority for the CALIPSO mission. For present purposes, we accept these differences as real and thereby apply separate daytime and nighttime calibration constants to estimate τ_{top}.

2.5.2.2. Effect of Opacity Flag

[41] The top row of Table 1 and Figure 3, top, show results when all screening criteria except the Opacity Flag are used, while the bottom row of Table 1 and Figure 3, bottom, include the Opacity Flag. This criterion eliminates 20% of the cases during the day (367 versus 459 cases) and 13% at night (805 versus 930 cases). Imposing the Opacity Flag criterion does not cause a dramatic shift in the mean values of any of the calibration constants, nor does it cause a substantial change in variability or detection limit for the CR method. On the other hand, there is a dramatic effect on both variability and detection limit for the DR method, especially during the day. The detection limit (DL) presented

in Table 2 is the minimum optical depth, τ_{top}, that can be detected with 99% confidence at 5-km resolution given the observed variability for unobstructed opaque clouds on the assumption that this variability is normally distributed. (For the CR method, calculating DL requires an assumed value of $\mathring{a}$, which was taken as 2.0.) Adding the Opacity Flag criterion causes a substantial reduction in the standard deviation of $\gamma'_{water,SS,unobstructed}$ (DR method), which translates into a substantially lower DL (Table 2). Specifically, DL for $\tau_{top,DR}$ drops from 0.12 to 0.10 at night and from 0.27 to 0.12 during the day. Figure 3 shows that the reduction in variability for the DR method is associated with removing outlier, i.e., low values from the PDF of $\gamma'_{water,SS,unobstructed}$.

2.5.2.3. DR Versus CR

[42] As shown in Table 2, detection limits for the CR method are somewhat lower than for the DR method under all conditions and are much less affected by the use of the Opacity Flag screening criterion. In this sense, the CR method appears to be a more sensitive and robust retrieval technique. However, this statement applies only to the retrieval of fine-mode aerosol optical depth, since the CR method (unlike the DR method) has little or no sensitivity to coarse-mode aerosol or to overlying cloud layers.

2.5.2.4. Ångström Exponent

[43] The final issue concerning systematic error involves the value of $\mathring{a}$ which must be assumed a priori in the retrieval of $\tau_{top,CR}$ (equation (8)). On the basis of Sun photometer and in situ measurements of biomass burning aerosols over southern Africa and South America [*Eck et al.*, 1999, 2001, 2003; *Holben et al.*, 2001; *Chand et al.*, 2006], we assume a best guess value of 2.0 with an uncertainty of +/−0.4, as shown in Table 1. This assumption will be tested in two ways (see section 3): by comparing optical depths derived from the DR and CR methods and by using the combined approach to estimate, rather than assume, $\mathring{a}$.

3. Results

3.1. Comparison of CR and DR Aerosol Optical Depths

[44] Figure 4 shows a comparison of $\tau_{top,DR}$ and $\tau_{top,CR}$ for the most polluted region (5–15°S, 0–10°E) and month (August 2006) of our study domain. Error bars represent 1σ uncertainties, calculated as described in section 2.5. For clarity, error bars are shown for every 30th data point. Figure 4, left and right, show nighttime and daytime data, respectively. Figure 4, bottom, shows results when all screening criteria are applied, while Figure 4, top, shows results when all criteria are applied except the Opacity Flag. Data where either the DR or CR method indicates values below the detection limit (see section 2.5.2 and Table 2) are not shown. The dashed lines show lines of constant Ångström exponent, which is a unique function of the ratio $\tau_{top,CR}/\tau_{top,DR}$ as seen by substitution of equation (8) for $\tau_{top,CR}$ into (9), i.e.,

$$\mathring{a} = -\frac{1}{\ln(2)} \ln\left(1 - \frac{3\tau_{top,CR}}{4\tau_{top,DR}}\right) \tag{11}$$

[45] Figure 4 demonstrates the importance of data screening. Without use of the Opacity Flag criterion (top), data points are scattered across the upper left portion of the panels, indicating the existence of above-cloud layers with low Ångström exponent. These might be interpreted as dust aerosol or thin cirrus. However, these points disappear when the target clouds are required to be opaque (Figure 4, bottom). Thus, the correct interpretation for these points is most likely retrieval error when the DR method is applied to thin or patchy clouds.

[46] In both Figures 4c and 4d, most of the data points, especially optically thick aerosol layers ($\tau_{top} > 0.5$), are located close to the line indicative of $\mathring{a} = 2$. This tends to justify our choice of $\mathring{a} = 2$ in the CR method for this situation where the aerosol type (biomass smoke) is well known. Further, it demonstrates good overall agreement between the two methods when τ_{top} is dominated by fine-mode aerosol.

[47] As indicated in Figure 4, optical depths greater than 1.5 were not observed over this highly polluted domain using either method. This raises the question of the upper detection limit (UDL) of τ_{top} retrieved by these methods. The UDL is certainly less than 3, since an optical depth of 3 would fully attenuate the lidar beam, preventing quantification of the reflectivity of the underlying target cloud. Figure 4 provides empirical evidence that the UDL may be about 1.5, since optical depths up to that value, but not higher, were detected. Improved knowledge of the UDL (and, more generally, the sensitivity of these methods to high values of τ_{top}) may come from CALIPSO validation studies currently underway.

[48] Finally, the results shown in Figure 4 confirm previous suggestions [*Keil and Haywood*, 2003] that substantial aerosol optical depths (i.e., greater than 0.3) occur quite commonly over marine stratiform clouds off the coast of southern Africa during the biomass burning season. Indeed, the CALIPSO observations indicate that above-cloud aerosol optical depths in this region frequently exceed 0.6. In the next section we examine the geographical and seasonal distribution of such elevated aerosol layers.

3.2. Seasonal and Geographical Distribution of Elevated Aerosol Layers

[49] Figure 5 displays the geographic distribution of optically thick fine-mode aerosol layers ($\tau_{top,CR} > 0.3$) detected using the CR method over the entire eastern Atlantic Ocean for each of the 6 months from June to November 2006. As in Figure 4, we calculate $\tau_{top,CR}$ using an Ångström exponent, $\mathring{a}$, of 2; however, the aerosol type (and thus the true value of $\mathring{a}$) is not well known over this entire domain. Indeed, there are indications that the true value of $\mathring{a}$ is well below 2 over some portions of the domain (see below and Figure 6). Thus, the values of $\tau_{top,CR}$ (indicated by the color scale in Figure 5) should be interpreted as an aerosol index, not as an estimate of aerosol optical depth. We expect this aerosol index to be closely related to fine-mode optical depth.

[50] Keeping in mind that adjacent orbit tracks are days or even weeks apart in time, the small-scale variability in Figure 5 highlights the considerable day-to-day variability in the optical properties at any location. This, in turn, underscores the importance of meteorological variability

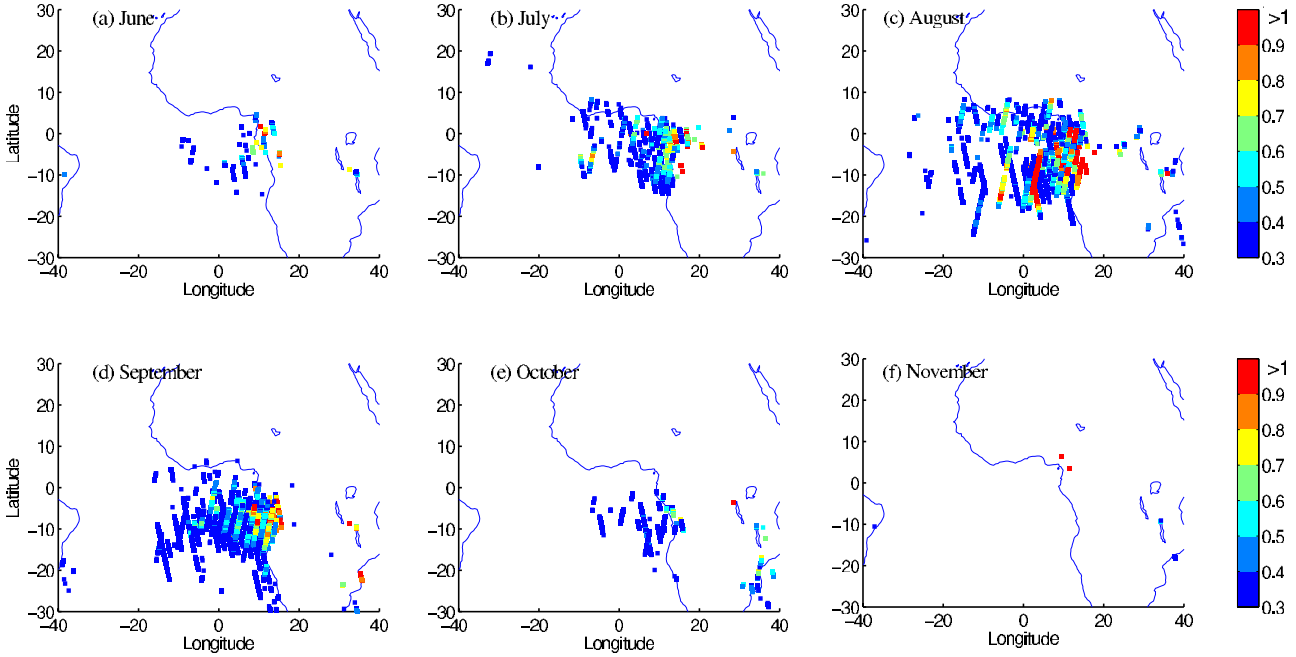

Figure 5. The geographical distribution of optically thick ($\tau_{top,CR} > 0.3$) aerosol layers overlying opaque clouds for the months of June–November 2006, based on the CR method. An Ångström exponent of 2 has been assumed even though the aerosol type is not, in fact, well known for the entire region. Thus, the values of $\tau_{top,CR}$ (indicated by the color scale) should be considered an aerosol index rather than an actual measure of aerosol optical depth. We expect this index to be closely related to the fine-mode optical depth. All available daytime and nighttime data are used, although calibration constants differ between day and night, as indicated in Table 2.

in determining the location and thickness of aerosol layers over the ocean to the west of southern Africa. Despite this small-scale noise, Figure 5 clearly shows the seasonal cycle of southern African biomass burning [*Ito et al.*, 2007] in that there is a much greater prevalence of optically thick, above-cloud aerosol layers during August and September than during other months. It is also impressive that these layers can be seen to extend over 4000 km downstream of the source regions. Detecting these extensive layers using clear-sky algorithms from passive satellite sensors would be hampered by the persistent cloud cover in this region and by the difficulties associated with screening out cloudy pixels.

[51] Figure 6 shows the Ångström exponent, *å*, for each suitable CALIPSO overpass during August 2006. The map indicates that å = 2.0 is a reasonable first approximation, especially near the region of most intense biomass burning aerosol. However, lower Ångström exponents (indicating larger particles) also occur, especially in the northeast portion of the domain (e.g., around 0°N and 10°E). These lower values may indicate the influence of Saharan dust aerosol or thin cirrus.

4. Conclusions and Recommendations

[52] A new approach that uses color ratio (CR) from spaceborne lidar is applied to the detection and characterization of aerosol layers overlying low clouds. The optical depth retrievals from this approach are compared with a previous method (the depolarization ratio method (DR), *Hu et al.* [2007a]), using CALIPSO Level-2 data off the coast of southern Africa, where biomass burning aerosols were frequently advected over marine stratiform clouds. Results indicate good agreement within estimated uncertainties. The CR method is most sensitive to fine-mode aerosols and essentially insensitive to thin clouds and coarse-mode dust. Because anthropogenic aerosol is predominantly found in the fine mode, the CR method can be used to identify situations where cloudy-sky anthropogenic forcing may be

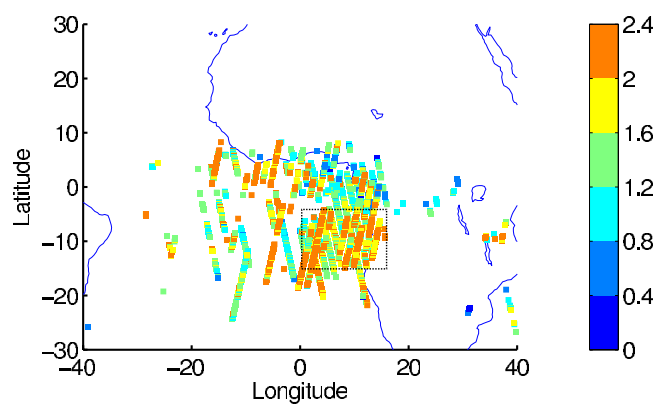

Figure 6. Map showing the Ångström exponent *å* (colors), derived using equation (9), of elevated aerosol layers above low opaque clouds during August 2006. Both daytime and nighttime data are used in this plot. The box shows the area with highest $\tau_{top,CR}$ and *å* just downwind of the major biomass burning region.

occurring. A combination of the DR and CR methods is shown to yield important information on the aerosol size (Ångström exponent). We demonstrate the capability of the CR method to detect elevated aerosol layers associated with biomass burning using 6 months of data from the southeast Atlantic. Layers with aerosol optical depth greater than 0.3 are commonly observed up to several thousand kilometers away from the source region over the Atlantic Ocean. The most geographically extensive and highest aerosol optical depths are observed during August and September 2006, with very few layers detected during November 2006.

[53] The prevalence and optical thickness of these aerosol layers above low marine boundary layer clouds have important implications for the regional radiation budget over the subtropical and tropical eastern Atlantic Ocean. Additionally, given that these aerosols are strongly absorbing [*Leahy et al.*, 2007], there are potentially important consequences for the atmospheric heating rates and lower atmospheric stability which may impact the formation of low clouds. Such layers have not previously been amenable to systematic measurement, e.g., using conventional remote methods such as surface-based Sun photometers or clear sky retrievals from passive satellite sensors.

[54] Examination of data from unobstructed low clouds allows empirical determination of calibration constants and calibration uncertainty for both methods. This, in turn, allows quantification of lower detection limits, which appear to be approximately 0.1 for aerosol optical depth at 532 nm for data aggregated to 5-km horizontal resolution. Both methods have an upper detection limit (UDL) as well, since too much aerosol attenuation will prevent accurate quantification of the reflectivity of the underlying target cloud. This study suggests that the UDL for both methods may be around an optical depth of 1.5. A related caveat, not previously mentioned, is the possibility that multiple scattering within the aerosol layer will artificially enhance the cloud top illumination within the detector field of view, causing an enhancement of apparent cloud reflectivity and an underestimation of aerosol optical depth. We expect this error to be negligible whenever the aerosol layer is vertically separated from the cloud layer, as is generally the case in the data examined herein. For aerosol layers directly above the target cloud layer, this could be a significant source of error. Quantification of these and other potential errors, as well as improved understanding of both the lower and upper detection limits, should be possible in the future using data from CALIPSO validation experiments currently in progress.

[55] Other types of validation studies are needed as well: for example, (1) studies of how the calibration constants vary with season and latitude and (2) studies that compare aerosol optical depth from these retrievals to the standard CALIPSO aerosol optical depth product (which will be available in the Version 2 data sets) and with MODIS retrievals of aerosol optical depth.

[56] Beyond validation work, CALIPSO-based estimates of above-cloud aerosol optical depth could be combined with MODIS-based estimates of the underlying cloud albedo and with in situ derived information on aerosol single scattering albedo in order to estimate the cloudy-sky DCF over the southeast Atlantic. Such estimates ought to provide a useful constraint for the evaluation of DCF in climate models.

[57] We find that while aerosol optical thickness estimates from the CR method are not strongly sensitive to inhomogeneities in the underlying cloud, those from the DR method are very sensitive. When the underlying cloud does not fully attenuate the lidar beam, the cloud target is unsuitable for use in retrieving aerosol optical depth with the DR method. This occurs for underlying clouds that are either thin or patchy (or both). We show that the Level-2 Opacity Flag can and should be used to screen data to ensure that only underlying clouds that fully attenuate the lidar beam are used for the DR retrieval method.

[58] We have demonstrated that both methods can be "self-calibrated" using observations from unobstructed low target clouds. Our analysis of 1 month of data from a remote oceanic region found substantially different calibration constants during the daytime and nighttime. One can anticipate that future implementations would benefit from studying orbit-to-orbit variations in the calibration constants and even latitudinal variations within individual orbits. Such studies should be possible given the prevalence of unobstructed low clouds around the globe and the ability of the CALIOP feature finder to identify these calibration targets.

[59] **Acknowledgments.** This work was supported by University of Washington startup funds, NASA's CALIPSO mission (contract NAS1-99105), the National Science Foundation (grants ATM-0601177 and ATM-0205198), and the NASA Goddard Earth Sciences and Technology program. We acknowledge the anonymous reviewers for their constructive comments.

References

Ångström, A. (1929), On the atmospheric transmission of Sun radiation and on dust in the air, *Geogr. Ann.*, *11*, 156–166, doi:10.2307/519399.

Beyerle, G., M. R. Gross, D. A. Haner, N. T. Kjome, I. S. McDermid, T. J. McGee, J. M. Rosen, H.-J. Schäfer, and O. Schrems (2001), A lidar and backscatter sonde measurement campaign at Table Mountain during February–March 1997: Observations of cirrus clouds, *J. Atmos. Sci.*, *58*, 1275–1287, doi:10.1175/1520-0469(2001)058<1275:ALABSM>2.0.CO;2.

Boucher, O., and T. L. Anderson (1995), General circulation model assessment of the sensitivity of direct climate forcing by anthropogenic sulfate aerosols to aerosol size and chemistry, *J. Geophys. Res.*, *100*(D12), 26,117–26,134, doi:10.1029/95JD02531.

Chand, D., P. Guyon, P. Artaxo, O. Schmid, G. P. Frank, L. V. Rizzo, O. L. Mayol-Bracero, L. V. Gatti, and M. O. Andreae (2006), Optical and physical properties of aerosols in the boundary layer and free troposphere over the Amazon Basin during the biomass burning season, *Atmos. Chem. Phys.*, *6*, 2911–2925.

Charlson, R. J., and M. J. Pilat (1969), Climate: The influence of aerosols, *J. Appl. Meteorol.*, *8*, 1001–1002, doi:10.1175/1520-0450(1969)008<1001:CTIOA>2.0.CO;2.

Chýlek, P., and J. A. Coakley (1974), Aerosols and climate, *Science*, *183*, 75–77, doi:10.1126/science.183.412075.

Eck, T., B. N. Holben, J. Reid, O. Dubovik, A. Smirnov, N. O'Neill, I. Slutsker, and S. Kinne (1999), Wavelength dependence of the optical depth of biomass burning, urban, and desert dust aerosols, *J. Geophys. Res.*, *104*(D24), 31,333–31,349, doi:10.1029/1999JD900923.

Eck, T., et al. (2001), Characterization of the optical properties of biomass burning aerosols in Zambia during the 1997 ZIBBEE field campaign, *J. Geophys. Res.*, *106*(D4), 3425–3448, doi:10.1029/2000JD900555.

Eck, T., et al. (2003), Variability of biomass burning aerosol optical characteristics in southern Africa during the SAFARI 2000 dry season campaign and a comparison of single scattering albedo estimates from radiometric measurements, *J. Geophys. Res.*, *108*(D13), 8477, doi:10.1029/2002JD002321.

Ensor, D. S., W. M. Porch, M. J. Pilat, and R. J. Charlson (1971), Influence of the atmospheric aerosol on albedo, *J. Appl. Meteorol.*, *10*, 1303–1306, doi:10.1175/1520-0450(1971)010<1303:IOTAAO>2.0.CO;2.

Haywood, J. M., and K. P. Shine (1997), Multi-spectral calculations of the direct radiative forcing of tropospheric sulphate and soot aerosols using a column model, *Q. J. R. Meteorol. Soc.*, *123*, 1907–1930, doi:10.1002/qj.49712354307.

Haywood, J. M., D. L. Roberts, A. Slingo, J. M. Edwards, and K. P. Shine (1997), General circulation model calculations of the direct radiative forcing by anthropogenic sulfate and fossil-fuel soot aerosol, *J. Clim.*, *10*, 1562–1577, doi:10.1175/1520-0442(1997)010<1562:GCMCOT>2.0.CO;2.

Holben, B. N., et al. (2001), An emerging ground-based aerosol climatology: Aerosol optical depth from AERONET, *J. Geophys. Res.*, *106*(D11), 12,067–12,097, doi:10.1029/2001JD900014.

Hu, Y., Z. Liu, D. Winker, M. Vaughan, V. Noel, L. Bissonnette, G. Roy, and M. McGill (2006), Simple relation between lidar multiple scattering and depolarization for water clouds, *Opt. Lett.*, *31*, 1809–1811, doi:10.1364/OL.31.001809.

Hu, Y., M. Vaughan, Z. Liu, K. Powell, and S. Rodier (2007a), Retrieving optical depths and lidar ratios for transparent layers above opaque water clouds from CALIPSO lidar measurements, *IEEE Trans. Geosci. Remote Sens. Lett.*, *4*, 523–526.

Hu, Y., et al. (2007b), The depolarization–attenuated backscatter relation: CALIPSO lidar measurements vs. theory, *Opt. Express*, *15*, 5327–5332, doi:10.1364/OE.15.005327.

Intergovernmental Panel of Climate Change (IPCC) (2007), *Climate Change 2007: The Physical Science Basis*, *Contribution of Working Group I to the Fourth Assessment Report of the IPCC*, Cambridge Univ. Press, New York.

Ito, A., A. Ito, and H. Akimoto (2007), Seasonal and interannual variations in CO and BC emissions from open biomass burning in southern Africa during 1998–2005, *Global Biogeochem. Cycles*, *21*, GB2011, doi:10.1029/2006GB002848.

Keil, A., and J. M. Haywood (2003), Solar radiative forcing by biomass burning aerosol particles during SAFARI 2000: A case study based on measured aerosol and cloud properties, *J. Geophys. Res.*, *108*(D13), 8467, doi:10.1029/2002JD002315.

Klein, S. A., and D. L. Hartmann (1993), The seasonal cycle of low stratiform clouds, *J. Clim.*, *6*, 1588–1606, doi:10.1175/1520-0442(1993)006<1587:TSCOLS>2.0.CO;2.

Leahy, L. V., T. L. Anderson, T. F. Eck, and R. W. Bergstrom (2007), A synthesis of single scattering albedo of biomass burning aerosol over southern Africa during SAFARI 2000, *Geophys. Res. Lett.*, *34*, L12814, doi:10.1029/2007GL029697.

Liu, Z., M. A. Vaughan, D. M. Winker, C. A. Hostetler, L. R. Poole, D. Hlavka, W. Hart, and M. McGill (2004), Use of probability distribution functions for discriminating between cloud and aerosol in lidar backscatter data, *J. Geophys. Res.*, *109*, D15202, doi:10.1029/2004JD004732.

Liu, Z., W. Hunt, M. A. Vaughan, C. A. Hostetler, M. McGill, K. Powell, D. Winker, and Y. Hu (2006), Estimating random errors due to shot noise in backscatter lidar observations, *Appl. Opt.*, *45*, 4437–4447, doi:10.1364/AO.45.004437.

McCubbin, I. B., et al. (2006), Overview of the multi-aircraft CALIPSO-CloudSat validation experiment, *Eos Trans. AGU*, *87*(52), Fall Meet. Suppl., Abstract A51E-0146.

McGill, M., D. Hlavka, W. Hart, V. S. Scott, J. Spinhirne, and B. Schmid (2002), The cloud physics lidar: Instrument description and initial measurement results, *Appl. Opt.*, *41*, 3725–3734, doi:10.1364/AO.41.003725.

O'Connor, E. J., A. J. Illingworth, and R. J. Hogan (2004), A technique for autocalibration of cloud lidar, *J. Atmos. Ocean. Technol.*, *21*, 777–786, doi:10.1175/1520-0426(2004)021<0777:ATFAOC>2.0.CO;2.

Pinnick, R. G., S. G. Jennings, P. Chýlek, C. Ham, and W. T. J. Grandy (1983), Backscatter and extinction in water clouds, *J. Geophys. Res.*, *88*(C11), 6787–6796, doi:10.1029/JC088iC11p06787.

Platt, C. M. R., D. M. Winker, M. A. Vaughan, and S. D. Miller (1999), Backscatter to extinction ratios in the top layers of tropical mesoscale convective systems and in isolated cirrus from LITE observations, *J. Appl. Meteorol.*, *38*, 1330–1345, doi:10.1175/1520-0450(1999)038<1330:BTERIT>2.0.CO;2.

Rossow, W. B., and R. A. Schiffer (1999), Advances in understanding clouds from ISCCP, *Bull. Am. Meteorol. Soc.*, *80*, 2261–2288, doi:10.1175/1520-0477(1999)080<2261:AIUCFI>2.0.CO;2.

Schulz, M., et al. (2006), Radiative forcing by aerosols as derived from the AeroCom present-day and pre-industrial simulations, *Atmos. Chem. Phys.*, *6*, 5225–5246.

Seinfeld, J. H., and S. N. Pandis (1998), *Atmospheric Chemistry and Physics: From Air Pollution to Climate Change*, Wiley Intersci., New York.

Stephens, G. L., R. J. Engelen, M. Vaughan, and T. L. Anderson (2001), Toward retrieving properties of the tenuous atmosphere using space-based lidar measurements, *J. Geophys. Res.*, *106*(D22), 28,143–28,157, doi:10.1029/2001JD000632.

Stephens, G. L., et al. (2002), The CloudSat mission and the A-Train, *Bull. Am. Meteorol. Soc.*, *83*, 1771–1790, doi:10.1175/BAMS-83-12-1771.

van de Hulst, H. C. (1981), *Light Scattering by Small Particles*, Dover Publ., New York.

Whitby, K. T., R. B. Husar, and Y. H. Liu (1972), The aerosol size distribution of Los Angeles smog, *J. Colloid Interface Sci.*, *39*, 177–204, doi:10.1016/0021-9797(72)90153-1.

Winker, D. M., J. Pelon, and M. P. McCormick (2002), The CALIPSO mission: Spaceborne lidar for observation of aerosols and clouds, *Proc. SPIE Soc. Opt. Eng.*, *4893*, 1–11.

Winker, D. M., W. H. Hunt, and M. J. McGill (2007), Initial performance assessment of CALIOP, *Geophys. Res. Lett.*, *34*, L19803, doi:10.1029/2007GL030135.

Young, S. A. (1995), Analysis of lidar backscatter profiles in optically thin clouds, *Appl. Opt.*, *34*, 7019–7031.

Yu, H., et al. (2005), A review of measurement-based assessment of aerosol direct radiative effect and forcing, *Atmos. Chem. Phys.*, *5*, 7647–7768.

T. L. Anderson, D. Chand, R. J. Charlson, and R. Wood, Department of Atmospheric Sciences, University of Washington, Box 351640, Seattle, WA 98195-1640, USA. (tadand@u.washington.edu; duli@u.washington.edu; bobwhan@comcast.net; robwood2@u.washington.edu)

Y. Hu and M. Vaughan, NASA Langley Research Center, Hampton, VA 23681, USA. (yongxiang.hu-1@nasa.gov; mark.a.vaughan@nasa.gov)

Z. Liu, National Institute of Aerospace, Hampton, VA 23666, USA. (zhaoyan.liu-1@nasa.gov)